Rayleigh–Taylor instability of multi-fluid layers in cylindrical geometry*

Hong-Yu Guo(郭宏宇)[1,2], Li-Feng Wang(王立锋)[2,3,†], Wen-Hua Ye(叶文华)[2,3,‡], Jun-Feng Wu(吴俊峰)[2], and Wei-Yan Zhang(张维岩)[2]

[1] *Graduate School, China Academy of Engineering Physics, Beijing* 100088, *China*
[2] *Institute of Applied Physics and Computational Mathematics, Beijing* 100094, *China*
[3] *HEDPS, Center for Applied Physics and Technology, Peking University, Beijing* 100871, *China*

(Received 27 July 2017; revised manuscript received 3 September 2017; published online 20 November 2017)

Rayleigh-Taylor instability of three fluid layers with two interfaces in cylindrical geometry is investigated analytically. The growth rates and the amplitudes of perturbation on the two interfaces are obtained. The feedback factor from outer to inner interface is larger than that from inner to outer interface under the same conditions. The growth rate on the initially unstable interface is larger than the corresponding result in planar geometry for low mode perturbation. The two interfaces are decoupled for a larger mode number perturbation. The dependencies of the amplitudes of perturbation on different initial conditions are analyzed. The negative feedback effect from initially stable interface to another unstable interface is observed. In the limit of infinity inner radius and finite shell thickness, the results in planar geometry are recovered.

Keywords: Rayleigh–Taylor instability, cylindrical geometry, inertial-confinement fusion implosions

PACS: 52.57.Fg, 47.20.Ma, 52.35.Py **DOI:** 10.1088/1674-1056/26/12/125202

1. Introduction

When a heavier fluid is accelerated by a lighter one, the perturbed interface between two fluids is Rayleigh-Taylor instability (RTI).[1,2] The RTI plays a significant role in many areas, such as astrophysics[3] and inertial confinement fusion (ICF).[4,5] In a typical ICF explosion experiment, the ignition capsule consisting of an ablator-fuel shell filled with a low density deuterium–tritium gas is directly irradiated by laser or indirectly irradiated by x-rays. The major issue plaguing the achievement of high-symmetry compression is the so called RTI.[5] It is necessary to maintain the integrity of the implosion shell during the entire implosion process. In the acceleration stage, the RTI can break up the implosion shell, causing the mixing of ablator material into the fuel material. In the deceleration stage, the RTI can cause seriously distortion of the hot-spot, even quenching the hot-spot, resulting in performance degradation of ICF implosions. Thus, the RTI growth must be controlled to an acceptable level and RTI remains a critical issue in the successful ICF implosions.

The classical RTI refers to a semi-infinite fluid of density ρ_1 supporting another semi-infinite fluid of density ρ_2 ($\rho_2 > \rho_1$) in a gravitational field. Small amplitude of perturbation on the interface will grow exponentially, $\eta(t) \sim \eta_0 e^{\gamma t}$, where $\gamma = \sqrt{Akg}$ is the linear growth rate of RTI growth, η_0 is the initial perturbation, $A = (\rho_2 - \rho_1)/(\rho_2 + \rho_1)$ is the Atwood number, k is wave number, and g is the acceleration. Based on this classical configuration of two semi-infinite fluids model, the RTI has been extensively studied analytically,[6–8] numerically,[9] and experimentally.[4,10] A single fluid layer accelerated by uniform pressure is first investigated by Taylor.[2] Mikaelian[11–13] extends the single fluid layer to the multi-layers model to study the density gradient stabilization effect where the continuous profile of density is approached by multi-finite-thickness fluids. In ICF implosion experiment, a relatively thin fuel shell is imploded inward. The finite-thickness effect and the coupling effect between the interfaces are very important during the implosion. The physics of "interface coupling" that means the evolution of small perturbation at one interface depends not only on its initial disturbance but also on the perturbations at the adjacent interfaces.[13–15] The thin shell will lead to much more severe RTI growth which can be seen in Ref.15 where the RTI in two finite-thickness fluids is discussed analytically. Recently, in a magnetized liner inertial fusion (MagLIF) experiment, Awe[16] found an embedded axial magnetic field may strengthen the integrity of the inner interface against magneto-Rayleigh–Taylor instability (MRTI). The MRTI properties of a finite slab are investigated by Weis,[17] the feedthrough may be reduced if there are magnetic fields on the two sides of the slab. The analytical work mentioned above is restricted to planar ge-

*Project supported by the National Natural Science Foundation of China (Grant Nos. 11275031, 11475034, 11575033, and 11274026) and the National Basic Research Program of China (Grant No. 2013CB834100).

†Corresponding author. E-mail: wang_lifeng@iapcm.ac.cn
‡Corresponding author. E-mail: ye_wenhua@iapcm.ac.cn

© 2017 Chinese Physical Society and IOP Publishing Ltd

ometry. However, in many cases like ICF implosions, RTI always occurs in non-Cartesian systems. The RTI growth in convergent geometry was first derived by Bell[18] and Plesset,[19] their results were collectively called as Bell–Plesset (BP) effects. It is found that the geometrical convergence can lead to the instability growth even without acceleration by considering BP effects.[20] Recently, a weakly nonlinear (WN) model for RTI growth in cylindrical[21] and spherical[22] geometry are established for incompressible fluids, respectively. All of these models are described by two fluids that separated by a single curved interface. In this paper, we discuss the RTI growth of multi-layers in cylindrical geometry. The growth rate and the evolution of perturbation are discussed in some detail.

This paper is organized as follows. In Section 2, the theoretical model is presented. Section 3 displays the result and discussion. Section 4 summarizes the major results.

2. Theoretical model

The theoretical model of the present work is introduced in this section. The cylindrical coordinate system is established where r and θ are, respectively, normal and along to the unperturbed interface between the fluids. Considering three cylindrical layers of two interfaces with R_1 to be inner radius and R_2 to be outer radius ($R_2 = R_1 + \Delta R$), ΔR is the thickness of the middle shell. The density of inner, middle and outer fluids are, respectively, $\rho_{\rm a}$ ($0 < r < R_1$), $\rho_{\rm b}$ ($R_1 < r < R_2$), and $\rho_{\rm c}$ ($R_2 < r < \infty$). The two perturbed interfaces of the three fluids are parameterized as $r = R_1 + \eta_{\rm i}(\theta,t)$ and $r = R_2 + \eta_{\rm o}(\theta,t)$ where $\eta_{\rm i}(\theta,t)$ and $\eta_{\rm o}(\theta,t)$ are the perturbation displacements at the inner and outer interface, respectively. Assuming the fluid layers in a gravitational field $\boldsymbol{g} = -g\hat{\boldsymbol{e}}_r$ (e.g., the hot-spot/fuel interface during the deceleration stage of ICF implosion) to be inviscid, irrotational, and incompressible, the governing equations can be expressed as

$$\frac{\partial \eta_{\rm i}}{\partial t} + \frac{1}{r^2}\frac{\partial \eta_{\rm i}}{\partial \theta}\frac{\partial \phi_{\rm a}}{\partial \theta} - \frac{\partial \phi_{\rm a}}{\partial r} = 0, \quad \text{at } r = R_1 + \eta_{\rm i}, \tag{1}$$

$$\frac{\partial \eta_{\rm i}}{\partial t} + \frac{1}{r^2}\frac{\partial \eta_{\rm i}}{\partial \theta}\frac{\partial \phi_{\rm b}}{\partial \theta} - \frac{\partial \phi_{\rm b}}{\partial r} = 0, \quad \text{at } r = R_1 + \eta_{\rm i}, \tag{2}$$

$$\rho_{\rm a}\left[\frac{\partial \phi_{\rm a}}{\partial t} + \frac{1}{2}\left(\frac{\partial \phi_{\rm a}}{\partial r}\right)^2 + \frac{1}{2r^2}\left(\frac{\partial \phi_{\rm a}}{\partial \theta}\right)^2 + gr\right] - \rho_{\rm b}\left[\frac{\partial \phi_{\rm b}}{\partial t} + \frac{1}{2}\left(\frac{\partial \phi_{\rm b}}{\partial r}\right)^2 + \frac{1}{2r^2}\left(\frac{\partial \phi_{\rm b}}{\partial \theta}\right)^2 + gr\right] + f_1(t) = 0, \quad \text{at } r = R_1 + \eta_{\rm i}, \tag{3}$$

$$\frac{\partial \eta_{\rm o}}{\partial t} + \frac{1}{r^2}\frac{\partial \eta_{\rm o}}{\partial \theta}\frac{\partial \phi_{\rm b}}{\partial \theta} - \frac{\partial \phi_{\rm b}}{\partial r} = 0, \quad \text{at } r = R_2 + \eta_{\rm o}, \tag{4}$$

$$\frac{\partial \eta_{\rm o}}{\partial t} + \frac{1}{r^2}\frac{\partial \eta_{\rm o}}{\partial \theta}\frac{\partial \phi_{\rm c}}{\partial \theta} - \frac{\partial \phi_{\rm c}}{\partial r} = 0, \quad \text{at } r = R_2 + \eta_{\rm o}, \tag{5}$$

$$\rho_{\rm b}\left[\frac{\partial \phi_{\rm b}}{\partial t} + \frac{1}{2}\left(\frac{\partial \phi_{\rm b}}{\partial r}\right)^2 + \frac{1}{2r^2}\left(\frac{\partial \phi_{\rm b}}{\partial \theta}\right)^2 + gr\right] - \rho_{\rm c}\left[\frac{\partial \phi_{\rm c}}{\partial t} + \frac{1}{2}\left(\frac{\partial \phi_{\rm c}}{\partial r}\right)^2 + \frac{1}{2r^2}\left(\frac{\partial \phi_{\rm c}}{\partial \theta}\right)^2 + gr\right] + f_2(t) = 0, \quad \text{at } r = R_2 + \eta_{\rm o}, \tag{6}$$

where $\phi_{\rm a}$, $\phi_{\rm b}$, and $\phi_{\rm c}$ are the velocity potentials that are related to the inner, middle and outer fluids, respectively. f_1 and f_2 are the arbitrary functions of time. Equations (1) and (2) represent the normal velocity is continuous across the inner interface. The pressure continuity condition (i.e., Bernoulli equation) across the inner interface is described by Eq. (3). The normal velocity and pressure are also continuous across the outer interface which are expressed by Eqs. (4)–(6). For a single-mode cosinusoidal perturbation, the small perturbation displacements $\eta_{\rm i}(\theta,t)$ and $\eta_{\rm o}(\theta,t)$ are written as

$$\eta_{\rm i}(\theta,t) = \eta_1(t)\cos(m\theta), \tag{7}$$

$$\eta_{\rm o}(\theta,t) = \eta_2(t)\cos(m\theta), \tag{8}$$

where m is the mode number. $\eta_1(t)$ and $\eta_2(t)$ are, respectively, the amplitudes of perturbation at inner and outer interfaces that we want to obtain. The velocity potentials describing the incompressible fluids are

$$\phi_n(r,\theta,t) = \phi^{(0)}(t) + \varphi_n(r,\theta,t), \tag{9}$$

where the subscript $n = {\rm a,b,c}$ represent the velocity potentials of three fluid layers. $\phi^{(0)}(t)$ is the unperturbed velocity potential and $\varphi_n(r,\theta,t)$ are the perturbed velocity potentials which can be expressed as

$$\varphi_{\rm a}(r,\theta,t) = d_1(t)r^m\cos(m\theta), \tag{10}$$

$$\varphi_{\rm b}(r,\theta,t) = [d_2(t)r^m + d_3(t)r^{-m}]\cos(m\theta), \tag{11}$$

$$\varphi_c(r,\theta,t) = d_4(t) r^{-m} \cos(m\theta), \tag{12}$$

as can be seen in Eqs. (10)-(12), $\varphi_n(r,\theta,t)$ related to the incompressible fluids satisfy the Laplace equation $\nabla^2\varphi_n = 0$ and the conditions $\nabla\varphi_a|_{r\to 0} = 0$ ($m \geq 2$) and $\nabla\varphi_c|_{r\to\infty} = 0$. Substituting Eqs. (7)–(12) into the governing equations (1)–(6), we can obtain six time-dependent equations. Eliminating the parameters $d_1(t)$, $d_2(t)$, $d_3(t)$, and $d_4(t)$, the coupled second-order ordinary differential equations (ODEs) for $\eta_1(t)$ and $\eta_2(t)$ are derived as

$$\frac{\mathrm{d}^2\eta_1}{\mathrm{d}t^2} - \frac{(1+A_1)\,\zeta^{-m+1}}{1+A_1\zeta^{-2m}}\frac{\mathrm{d}^2\eta_2}{\mathrm{d}t^2} - A_1\frac{m}{R_1}g\frac{1-\zeta^{-2m}}{1+A_1\zeta^{-2m}}\eta_1 = 0, \tag{13}$$

$$\frac{\mathrm{d}^2\eta_2}{\mathrm{d}t^2} - \frac{(1-A_2)\,\zeta^{-m-1}}{1-A_2\zeta^{-2m}}\frac{\mathrm{d}^2\eta_1}{\mathrm{d}t^2} - A_2\frac{m}{R_2}g\frac{1-\zeta^{-2m}}{1-A_2\zeta^{-2m}}\eta_2 = 0, \tag{14}$$

where $\zeta = R_2/R_1$ is the ratio of the outer radius to the inner radius. $A_1 = (\rho_b - \rho_a)/(\rho_b + \rho_a)$ and $A_2 = (\rho_c - \rho_b)/(\rho_c + \rho_b)$ are the Atwood numbers at inner and outer interface, respectively. Using the most common initial conditions, $\eta_1(t=0) = \varepsilon_1$, $\mathrm{d}\eta_1(t=0)/\mathrm{d}t = \dot{\varepsilon}_1$, $\eta_2(t=0) = \varepsilon_2$, and $\mathrm{d}\eta_2(t=0)/\mathrm{d}t = \dot{\varepsilon}_2$, the temporal evolution of the perturbations η_1 and η_2 can be obtained by solving the coupled ODEs. The results are

$$\begin{aligned}\eta_1(t) = \frac{1}{1-C_{12}C_{21}}\Big\{&\left[\varepsilon_1 - C_{21}\varepsilon_2\right]\cosh(\gamma_1 t) + C_{21}\left[\varepsilon_2 - C_{12}\varepsilon_1\right]\cosh(\gamma_2 t)\\ &+\frac{1}{\gamma_1}\left[\dot{\varepsilon}_1 - C_{21}\dot{\varepsilon}_2\right]\sinh(\gamma_1 t) + \frac{1}{\gamma_2}C_{21}(\dot{\varepsilon}_2 - C_{12}\dot{\varepsilon}_1)\sinh(\gamma_2 t)\Big\},\end{aligned} \tag{15}$$

$$\begin{aligned}\eta_2(t) = \frac{1}{1-C_{12}C_{21}}\Big\{&\left[\varepsilon_2 - C_{12}\varepsilon_1\right]\cosh(\gamma_2 t) + C_{12}\left[\varepsilon_1 - C_{21}\varepsilon_2\right]\cosh(\gamma_1 t)\\ &+\frac{1}{\gamma_2}\left[\dot{\varepsilon}_2 - C_{12}\dot{\varepsilon}_1\right]\sinh(\gamma_2 t) + \frac{1}{\gamma_1}C_{12}\left[\dot{\varepsilon}_1 - C_{21}\dot{\varepsilon}_2\right]\sinh(\gamma_1 t)\Big\},\end{aligned} \tag{16}$$

as can be seen in Eqs. (15) and (16), the perturbations at two interfaces are coupled each other, especially for a thin shell. The physics of coupling effect between two interfaces are represented by the coefficients C_{12} and C_{21}. The feedback coefficient of perturbation from inner surface to the outer surface is represented by C_{12}, that from outer surface to inner surface is described by C_{21}. It is well known that the RTI growth of a thin shell is much more severe than a thick shell.[14] The growth rate γ_1 and γ_2 are expressed as

$$\bar{\gamma}_1^2 = \frac{\gamma_1^2}{gm/R_1} = \frac{-b+\sqrt{b^2-4ac}}{2a}, \tag{17}$$

$$\bar{\gamma}_2^2 = \frac{\gamma_1^2}{gm/R_1} = \frac{-b-\sqrt{b^2-4ac}}{2a}, \tag{18}$$

where the coefficients a, b, and c depend only on the ratio of radius ζ, Atwood number A_1, A_2, and the mode number m:

$$a = 1 + A_1A_2\zeta^{-2m}, \tag{19}$$

$$b = A_1A_2\zeta^{-2m}\left(1-\zeta^{-1}\right) - A_2\zeta^{-1} - A_1, \tag{20}$$

$$c = A_1A_2\zeta^{-1}\left(1-\zeta^{-2m}\right), \tag{21}$$

As observed by Mikaelian[12] in planar geometry, the growth rates are invariant under the condition $\rho_b \to \rho_a\rho_c/\rho_b$ (interchanging the Atwood numbers at two interfaces). This interesting symmetry can be easily understood with a simple example, the two growth rates for the density profile (ρ_a, ρ_b, ρ_c) = (1, 10, 20) are identical to that of (1, 2, 20) for all perturbation wavelengths. However, this symmetrical property is not exist in cylindrical geometry which can be seen in Eqs. (17)–(21). If we interchange the values of A_1 and A_2, the values of two growth rates are all changed. When the middle shell becomes thicker enough ($\Delta R \to \infty$), the two interfaces are decoupled. Then, the growth rates of perturbations on two interfaces are, respectively

$$\begin{aligned}\gamma_1(\Delta R\to\infty) &= \sqrt{A_1\frac{m}{R_1}g},\\ \gamma_2(\Delta R\to\infty) &= \sqrt{A_2\frac{m}{R_2}g},\end{aligned} \tag{22}$$

which is consistent with the result of a single perturbed interface in cylindrical geometry.[21] For a much thinner shell ($\Delta R \to 0$), the growth rate is reduced to $\gamma = \sqrt{Amg/R}$ which is identical to result in cylindrical RTI[21] with $R_1 = R_2 \equiv R$ and $A = (\rho_c - \rho_a)/(\rho_c + \rho_a)$. The coefficients C_{12} and C_{21} are expressed as

$$C_{12} = \frac{\bar{\gamma}_1^2(1-A_2)\,\zeta^{-m-1}}{\bar{\gamma}_1^2(1-A_2\zeta^{-2m}) - A_2\zeta^{-1}(1-\zeta^{-2m})}, \tag{23}$$

$$C_{21} = \frac{\bar{\gamma}_2^2(1+A_1)\,\zeta^{-m+1}}{\bar{\gamma}_2^2(1+A_1\zeta^{-2m}) - A_1(1-\zeta^{-2m})}, \tag{24}$$

where the explicit A_2 and m dependencies of C_{12} and explicit A_1 and m dependencies of C_{21} are displayed clearly. The cou-

pling factor of two interfaces of finite-thickness slab[14] is represented by e^{-kd} which is quite different from the result in cylindrical case, where k is the wave number and d is the thickness of the fluid. It is interesting to note that the amplitude of perturbation in cylindrical geometry should reduce to that in planar geometry for quite short-wavelength perturbation compared to the inner radius R_1, namely, for the equivalent wavelength $\tilde{\lambda} = 2\pi R_1/m \ll R_1$. The equivalent wave number is defined as $\tilde{k} = m/R_1$ in cylindrical geometry.[21] That is to say, the RTI growth in cylindrical geometry is similar to that in planar geometry for larger mode number perturbation. Then, in the limit of infinite inner radius $R_1 \to \infty$ and finite shell thickness $\Delta R \ll R_1$, we have

$$\zeta^{-m} = \left(\frac{R_2}{R_1}\right)^{-m} = \left(1+\frac{\Delta R}{R_1}\right)^{-\tilde{k}R_1} \sim e^{-\tilde{k}\Delta R}, \qquad (25)$$

where the formula $\lim_{x\to\infty}(1+1/x)^x \sim e$ is used for the approximation. Using Eq. (25), the growth rate of the RTI and the amplitude of perturbation [Eqs. (15)–(18)] in cylindrical case is reduced to that in planar geometry.[13]

As observed in Eqs. (15) and (16), the amplitudes of the perturbation contain one growing mode with growth rate γ_1 and another growing mode with growth rate γ_2 which represent the intrinsic growth of the perturbations at the corresponding interfaces, where the two interfaces are initiated by the single-mode interface and the velocity perturbations. If we set $\varepsilon_1 = C_{21}\varepsilon_2$ and $\dot{\varepsilon}_1 = C_{21}\dot{\varepsilon}_2$, the growing modes of the growth rate γ_1 on both interfaces will be absent. Likewise, if $\varepsilon_2 = C_{12}\varepsilon_1$ and $\dot{\varepsilon}_2 = C_{12}\dot{\varepsilon}_1$, the growing modes of the growth rate γ_2 on two interfaces are completely suppressed. Moreover, it is found that suppressing any one of the growing mode on the one interface will automatically cancel the same mode on the other interface.

3. Results and discussion

In this section, we will study the growth rates of RTI and amplitudes of perturbations of multi-fluids in cylindrical geometry. The physical understanding of coupling effects between two curved interfaces is also discussed.

During the deceleration stage of ICF implosions, the outer surface of an implosion shell is stable, while the inner surface is RTI instable. The dependencies of coefficients C_{21} and C_{12} on Atwood number A_1 and A_2 for arbitrary R_2/R_1 are displayed in Fig. 1. The feedback coefficients decrease with increasing R_2/R_1, as the perturbation among the interfaces decays quickly when the shell becomes thick. As illustrated in Fig. 1(a), the feedback factor C_{21} from outer interface to inner interface is greatly affected by the A_2 on the outer interface. For fixed $A_1 = 0.9$, the value of C_{21} for $A_2 = -0.9$ is larger than that for $A_2 = -0.1$. However, the value of C_{21} for $A_1 = 0.9$ on the inner interface is a little larger than that for $A_1 = 0.1$ for fixed A_2. When A_2 on the outer interface tends to -1.0, the approximation $C_{21} \sim (R_2/R_1)^{-m+1}$ can be obtained for arbitrary mode number m. The C_{12} represents the feedback factor from inner interface to outer interface is influenced by A_1 on the inner interface which can be seen in Fig. 1(b). The larger A_1 is, the larger C_{12} will be for fixed R_2/R_1. The C_{12} has little dependence on A_2. When A_1 tends to 1.0, the approximation formula $C_{12} \sim (R_2/R_1)^{-m-1}$ is also obtained. Under the same conditions, the C_{21} (from outer interface to inner interface) is larger than C_{12} (from inner interface to outer interface) which is different from that in a planar slab,[14] where the feedback factor between two interfaces is e^{-kd}.

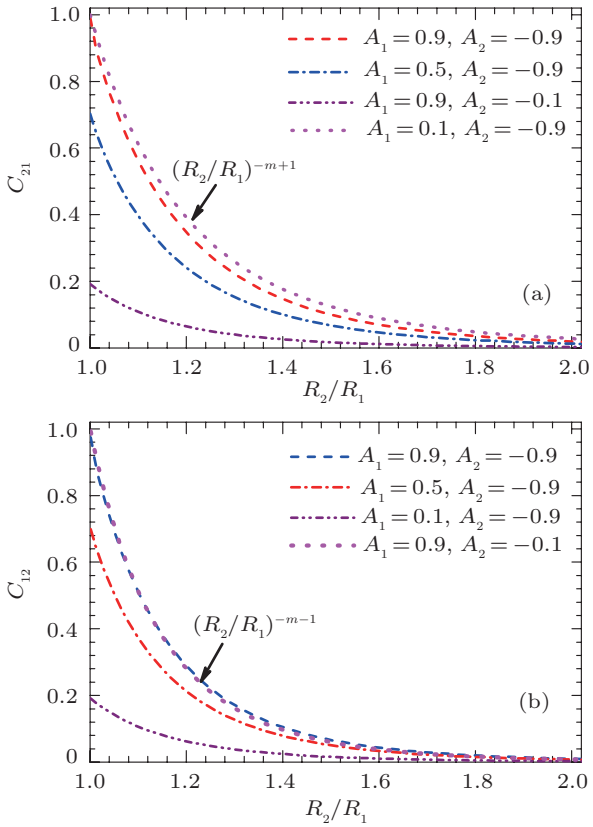


Fig. 1. (color online) The feedback coefficients C_{21} (a) and C_{12} (b) versus the ratio of the radius R_2/R_1 for different Atwood numbers A_1 and A_2 on two interfaces. The mode number $m = 6$. The line $(R_2/R_1)^{-m+1}$ is also plotted for comparison.

The mode number m dependence of the feedback coefficients C_{21} and C_{12} for Atwood numbers $A_1 = 0.9$ and $A_2 = -0.9$ are displayed in Fig. 2. With the increasing mode number m, the feedback coefficients C_{21} and C_{12} decrease quickly for the fixed R_2/R_1 which is shown in Fig. 2. This is because the coupling effect is severe for the large wave-length (low mode m) perturbation. For the lower mode perturbation, the coefficient C_{21} is larger than C_{12}. However, the C_{21} is approximated to the C_{12} for higher mode perturbation that is consistent with result in the planar case.[14,15]

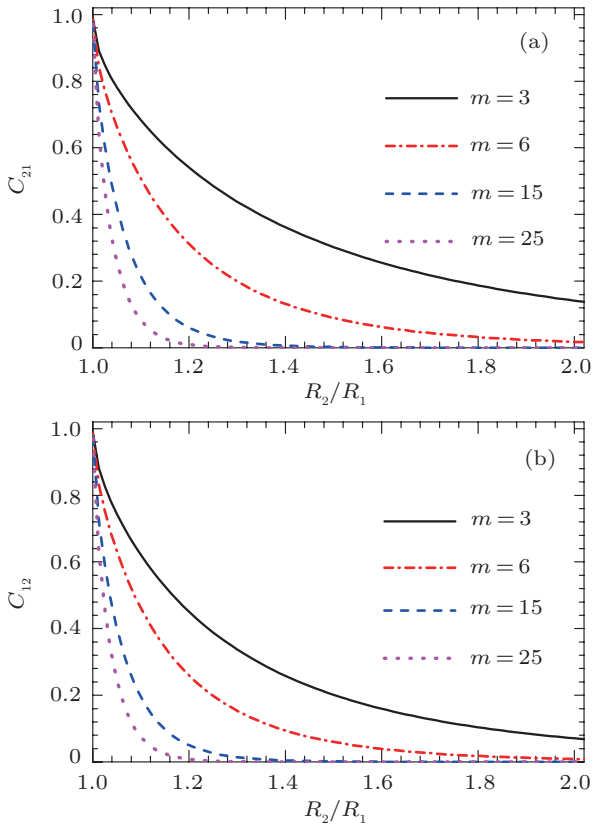


Fig. 2. (color online) The feedback coefficients C_{21} (a) and C_{12} (b) versus the ratio of radius R_2/R_1 for different mode number m. The Atwood numbers on the two interfaces are $A_1 = 0.9$ and $A_2 = -0.9$.

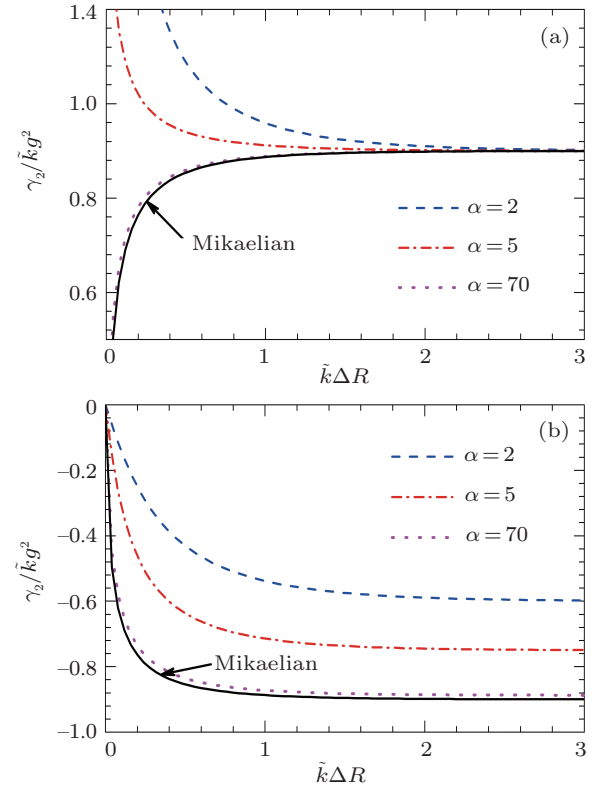


Fig. 3. (color online) The normalized growth rates of the perturbation $\gamma_1^2/\tilde{k}g$ (a) and $\gamma_2^2/\tilde{k}g$ (b) plotted against the normalized shell thickness $\tilde{k}\Delta R$ for $\alpha = 2, 5, 70$. The $\tilde{k} = m/R_1$ is the equivalent wave number in cylindrical geometry. The Atwood numbers $A_1 = 0.9$ and $A_2 = -0.9$. The Mikaelian's planar results[12] is also plotted for comparison.

In the implosion process, the in-flight aspect ratio (IFAR) is defined as the ratio of the imploded shell radius R_1 to its thickness ΔR, namely, $\alpha = R_1/\Delta R$. The RTI growth imposes an upper limit on the IFAR.[4] The normalized growth rates $\gamma_1^2/\tilde{k}g$ and $\gamma_2^2/\tilde{k}g$ of the RTI perturbation against the normalized thickness $\tilde{k}\Delta R$ are plotted in Fig. 3 for different α. The normalized $\gamma_1^2/\tilde{k}g$ decreases to the minimum (~ 0.9) with the increasing normalized shell thickness $\tilde{k}\Delta R$ for small α. For larger α, the behavior of the $\gamma_1^2/\tilde{k}g$ is a little different that grows to the maximum with $\tilde{k}\Delta R$. As shown in Fig. 3(a), the Mikaelian's results in the planar geometry[12] are recovered for $\alpha = 70$. During the deceleration stage, the outer interface of the shell is stable. As can be seen in Fig. 3(b), the $\gamma_2^2/\tilde{k}g$ is negative which represents the frequency of perturbation. With the increasing $\tilde{k}\Delta R$, the absolute value of $\gamma_2^2/\tilde{k}g$ increases to a maximum value. The absolute value of $\gamma_2^2/\tilde{k}g$ increases with increasing α. When $\alpha = 70$, Mikaelian's result for the frequency of perturbation in planar case is also recovered.[12]

Figure 4 displays the temporal evolution of the normalized amplitudes of perturbations $\tilde{k}\eta_1$ (perturbation at the inner interface) and $\tilde{k}\eta_2$ (perturbation at the outer interface) initiated by only interface perturbation in cylindrical geometry. The Atwood numbers at the two interfaces are $A_1 = 0.9$ and $A_2 = -0.9$. In Fig. 4(a), the normalized amplitudes of perturbations on the two interfaces are perturbed by only the inner interface perturbation with initial conditions $\varepsilon_1 = 0.001\tilde{\lambda}$ and $\varepsilon_2 = 0$ for mode number $m = 3, 10$. The $\tilde{\lambda} = 2\pi/\tilde{k}$ is the equivalent wavelength. The amplitude of perturbation η_1 on the inner interface is larger than η_2 on the outer interface for fixed normalized time $(\tilde{k}g)^{1/2}t$ and mode number m. The amplitude of perturbation η_1 for $m = 3$ is a little larger than that for $m = 10$ on the inner interface. For a small mode number m, the two interfaces are coupled. The perturbation on the inner interface feedback to the outer interface and the η_2 grows quickly for $m = 3$. However, the η_2 becomes negligibly small comparing to η_1 for $m = 10$, as the feedback effect become weak for large mode number. In Figure 4(b), a small perturbation is initially imposed only on the outer interface and the inner interface is kept undisturbed, namely, $\varepsilon_1 = 0$ and $\varepsilon_2 = 0.001\tilde{\lambda}$. The phase of perturbations are shifted by π in comparison to the initially cosinusoidal perturbation on the outer interface. The perturbation on the outer interface couples to the inner interface. Then, the amplitude of perturbation on the inner interface grows quickly as the inner interface is RTI unstable. For $m = 10$, the coupling effect becomes weak. The perturbation on the outer interface oscillates with time. With the time proceeding, the amplitude of perturbation on the inner face is larger than that on the outer interface, as the inner interface is subject to RTI. As shown in Fig. 4(c), both the inner and the

outer interface are initially perturbed with $\varepsilon_1 = \varepsilon_2 = 0.001\tilde{\lambda}$. The perturbations on the inner interfaces grow gradually with time. But the perturbations on the outer interface oscillate with time at the first, then grow quickly with time. As illustrated in Fig. 4(b), the perturbation from outer interface to the inner interface will cause the phase of the perturbations changing by π. That means the negative feedback effect from outer stable interface to inner unstable interface. The smaller mode number m is, the larger coefficient C_{21} will be. Thus, the amplitude of η_1 with $m = 3$ is smaller than that with $m = 10$.

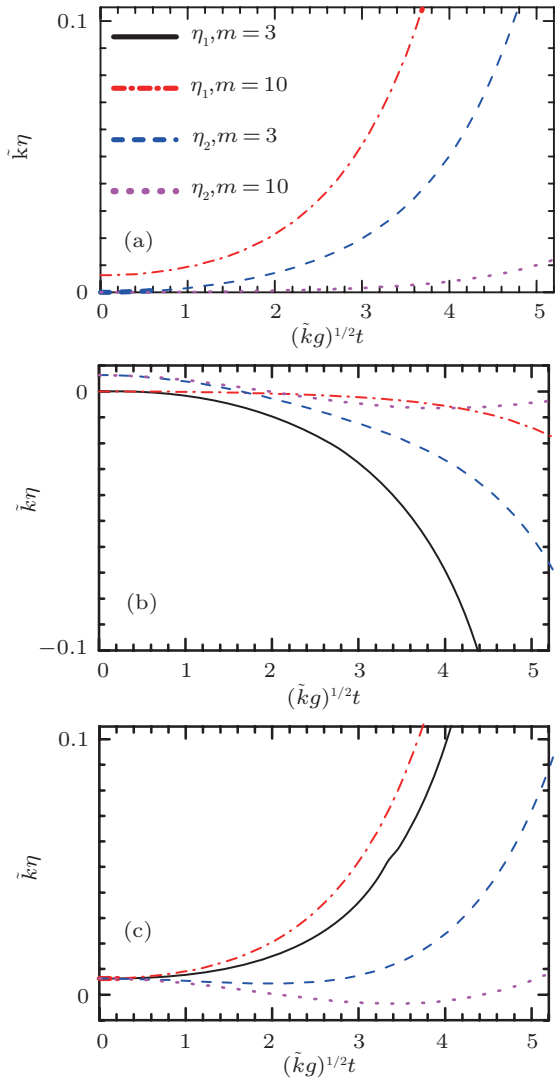


Fig. 4. (color online) Temporal evolution of the normalized amplitudes of perturbation $\tilde{k}\eta_1$ and $\tilde{k}\eta_2$ initialed by only the inner interface perturbation (a), only the outer interface perturbation (b), and both the inner and outer interface perturbations, respectively, for mode number $m = 3$ and 10 at $\zeta = 1.4$.

4. Conclusion

In this paper, the RTI growth on the two interfaces of three fluids in cylindrical geometry is studied analytically. The growth rate and the evolution of perturbations on the two interfaces are obtained. The feedback factor C_{21} (from outer to inner interface) is larger than C_{12} (from inner to outer interface) under the same condition. The larger mode number m leads to the smaller C_{12} (C_{21}). That means the two interfaces are decoupled for large mode number perturbation. The growth rate on the two interfaces are compared with Mikaelian's planar case.[12] Under the conditions of $\Delta R \ll R_1$ and $R_1 \to \infty$, Mikaelian's result for RTI growth of multi-layers is recovered. The dependencies of RTI on the different initial conditions are discussed. It is found the amplitudes of the perturbation on the two interfaces are shift by π when the outer interface is initially perturbed. The present result is respected to bring further understanding of RTI growth of multi-fluids in cylindrical geometry and to be probably significant for the assessment of the RTI in ICF implosions.

Acknowledgment

The author (Hong-Yu Guo) wishes to thank Prof. Xian-Tu He for his useful discussion and help.

References

[1] Rayleigh L 1883 *Proc. London Math. Soc.* **14** 170
[2] Taylor G 1950 *Proc. R. Soc. Lond. A* **201** 192
[3] Remington B A, Drake R P and Ryutov D D 2006 *Rev. Mod. Phys.* **78** 755
[4] Lindl J D, Amendt P, Berger R L, Glendinning S G, Glenzer S H, Haan S W, Kauffman R L, Landen O L and Suter L J 2004 *Phys. Plasmas* **11** 339
[5] Wang L F, Ye W H, He X T, Wu J F, Fan Z F, Xue C, Guo H Y, Miao W Y, Yuan Y T, Dong J Q, Jia G, Zhang J, Li Y J, Liu J, Wang M, Ding Y K and Zhang W Y 2017 *Sci. China-Phys. Mech. Astron.* **60** 055201
[6] Guo H Y, Yu X J, Wang L F, Ye W H, Wu J F and Li Y J 2014 *Chin. Phys. Lett.* **31** 044702
[7] Guo H Y, Wang L F, Ye W H, Wu J F and Zhang W Y 2017 *Chin. Phys. Lett.* **34** 045201
[8] Garnier J, Raviart P A, Clèrouin C C and Masse L 2003 *Phys. Rev. Lett.* **90** 185003
[9] Ye W H, Zhang W Y and He X T 2002 *Phys. Rev. E* **65** 057401
[10] Hsing W W and Hoffman N M 1997 *Phys. Rev. Lett.* **78** 3876
[11] Mikaelian K O 1982 *Phys. Rev. Lett.* **48** 1365
[12] Mikaelian K O 1982 *Phys. Rev. A* **26** 2140
[13] Mikaelian K O 1983 *Phys. Rev. A* **28** 1637
[14] Wang L F, Guo H Y, Wu J F, Ye W H, Liu J, Zhang W Y and He X T 2014 *Phys. Plasmas* **21** 122710
[15] Guo H Y, Wang L F, Ye W H, Wu J F and Zhang W Y 2017 *Chin. Phys. Lett.* **34** 075201
[16] Awe T J, McBride R D, Jennings C A, Lamppa D C, Martin M R, Rovang D C, Sinars D B, Slutz S A, Owen A C, Tomlinson K, Gomez M R, Hansen S B, Herrmann M C, McKenney J L, Robertson G K, Rochau G A, Savage M E, Schroen D G and Stygar W A 2014 *Phys. Plasmas* **21** 056303
[17] Weis M R, Zhang P, Lau Y Y, Rittersdorf I M, Zier J C, Gilgenbach R M, Hess M H and Peterson K J 2014 *Phys. Plasmas* **21** 122708
[18] Bell G I 1951 *Los Alamos National Laboratory Report* LA 1321
[19] Plesset M S 1954 *J. Appl. Phys.* **25** 96
[20] Wang L F, Wu J F, Guo H Y, Ye W H, Liu J, Zhang W Y and He X T 2015 *Phys. Plasmas* **22** 082702
[21] Wang L F, Wu J F, Ye W H, Zhang W Y and He X T 2013 *Phys. Plasmas* **20** 042708
[22] Zhang J, Wang L F, Ye W H, Wu J F, Guo H Y, Zhang W Y and He X T 2017 *Phys. Plasmas* **24** 062703